Chapter 4
Microrobots for Active Object Manipulation

Roel S. Pieters, Hsi-Wen Tung, and Bradley J. Nelson

Abstract Active manipulation of objects that are smaller than 1 mm in size finds its application in tasks such as assembly and pick-and-placement. Here, we present the design of a family of microrobots capable of object manipulation in a fluidic environment. The microrobots are fabricated from polymer (SU-8) with internal soft-magnetic posts (CoNi) that align to an external magnetic field and have a maximum dimension of $50 \times 200 \times 600\,\mu$m. Actuation of the device can be enforced with either a rotating or stepping magnetic field and corresponds to the method of object manipulation. In particular, a rotating magnetic field enables a fluidic-based noncontact manipulation technique, while a stepping magnetic field enables a contact manipulation technique. The capabilities of these designs are analysed and demonstrated with respect to the generated motion and the manipulation of objects.

Keywords Microrobot • Object manipulation • Magnetic actuation • Rolling actuation • Stepping actuation • Magnetic torque • Fluidic trapping • Fluidic drag • Fabrication • MEMS • Low Reynolds number • Microrobot design • Micromanipulation

1 Introduction

The manipulation of objects or components at the micrometer scale is a challenging task. As objects become smaller, disturbances come into play that can usually be ignored for the manipulation of objects with a larger size. Examples include effects due to surface interaction (e.g. Van der Waals force and electrostatics [1]) and the dominance of viscous forces when the surrounding environment is fluidic (e.g. water [2, 3]). Most commonly, locomotion of such untethered microdevices is either executed on a planar surface or in full 3D. The design (i.e. size, shape and actuation mechanism) of the device therefore prescribes its motion capabilities and the disturbances that will act upon it. When the size of the end-effector has

R.S. Pieters (✉) • H.-W. Tung • B.J. Nelson
Institute of Robotics and Intelligent Systems, ETH Zurich, Tannenstrasse 3, Zurich 8092, Switzerland
e-mail: rpieters@ethz.ch; bnelson@ethz.ch

D. Zhang, B. Wei (eds.), *Advanced Mechatronics and MEMS Devices II*, Microsystems and Nanosystems, DOI 10.1007/978-3-319-32180-6_4

the same order of magnitude as the size of the object, in general, manipulation becomes easier. Considering the microrobot as an end-effector, object manipulation differs greatly compared to manipulation with larger tools such as robotic tweezers or probes. Such tweezers are usually inserted from a certain angle and are limited in dexterity and degrees of freedom for manipulation. Moreover, when the size of the microrobot decreases, so does the force necessary for actuation. For instance, the drag force acting on a sphere in viscous flow scales with R, the radius of the sphere, while the gravitational force scales with the volume of the sphere, and thus with R^3. Additionally, when the object scales down such that the Reynolds number $Re \ll 1$, the motion of the microrobot and of objects will be more damped, and local fluidic effects can be exploited. In particular this includes the creation of a vortex due to the local rotation of the microrobot and a fluid's no-slip condition on the surface. Both can be used to aid in the lifting and/or transportation of objects. All these characteristics enable actuation techniques unconventional for macro-scale robotics and include magnetic, optical and fluidic techniques.

1.1 Related Work

Many different tools, designs and actuation techniques exist for micro- and nanomanipulation (see, e.g., [4]). A comparison regarding magnetically actuated microrobots can be found in [5, 6]. Moreover, a review on methods in automated planning and control for micromanipulation, and contact micromanipulation in particular can be found in [7, 8], respectively. Propulsion mechanisms with magnetic fields can be classified by the way energy is transferred to the robot, either force based with magnetic field gradients or torque based with alignment to a magnetic field. Examples of magnetic gradient control can be found in [5, 9, 10], while torque-based actuation techniques can be found in [3, 11, 12].

Regarding the manipulation of objects, research and applications in the microscale are single cell studies [13], minimally invasive surgery [14] and micro-assembly [15]. Other work considering manipulation using an untethered microrobot can be found in [12, 16]. Automated manipulation via fluidic trapping (i.e. pick-and-place) of beads with a similar microrobot as presented in this work is demonstrated in [17]. Additional work considering similar automated fluidic trapping strategies can be found in [16].

1.2 Micromanipulation Environment

Microrobot and micro-object manipulation is often executed in a low Reynolds number fluid environment. In this regime viscous forces are dominant and have to be overcome to achieve motion. Particular details of fluid mechanics at low Reynolds number can be found in many textbooks [18]. Other work, describing

life at low Reynolds number and robotics at the microscale can be found in [1, 2], respectively. One important effect that a low Reynolds number fluid has on bodies is the considerable influence of drag. When in motion, a translating and rotating body will be disturbed by a drag force and drag torque, respectively. This drag force and torque increases with increasing linear and rotational velocity of the body and with the viscosity of the surrounding medium. Other effects that occur due to the size scale are surface interaction forces such as adhesion or Van der Waals forces [19].

One additional property of a low Reynolds number flow that is worth mentioning is its reversibility. When $\mathrm{Re} \ll 1$, meaning a laminar and reversible flow, the microrobot can move forwards and backwards and have an almost instantaneous flow reversal. This means that when an object is transported without contact in the vortex, a sudden motion reversal of the robot will not result in the loss of the object.

In this chapter we present a family of microrobots that are actuated via torque with a rotating and stepping magnetic field. Additionally, we show the object manipulation capabilities of these microrobot designs. The rotating magnetic field enables a fluidic-based noncontact manipulation technique, while a stepping magnetic field enables a contact manipulation technique. We emphasize that these different robotic designs result in different actuation techniques and object manipulation approaches, while the fabrication process remains the same. By altering the internal and external configuration of the microrobot, that is, by changing the size, shape and configuration of the internal soft-magnetic posts with respect to the microrobot's body, entirely different propulsion and manipulation mechanisms are possible.

2 Microrobot Design

The microrobot (see Fig. 4.1 and Table 4.1) is a wireless mobile device and has a width of 60–200 µm and a length of 150–600 µm. It is designed as a cuboid (SU-8) with internal soft-magnetic posts consisting of a cobalt–nickel (CoNi) alloy that aligns with an external magnetic field. When the field direction changes, the microrobot realigns with it [20].

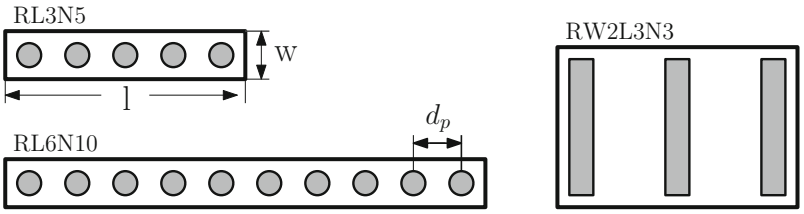

Fig. 4.1 Top view of the microrobot design. The geometry of the microrobot is defined by the length l and width w of the body. The configuration of the soft-magnetic posts differs in pitch between the posts d_p and the number of posts n_p. All cylindrical soft-magnetic posts have a diameter $D = 30\,\mu\mathrm{m}$ and a height of $h = 50\,\mu\mathrm{m}$. The *grey area* depicts CoNi, the white area depicts SU-8. The type description of the device is explained in Table 4.1

Table 4.1 Microrobot design configuration

Name	Rod length l µm	Rod width w µm	Post pitch d_p µm	Number of posts n_p
RL3N5	300	60	$2D$	5
RL6N10	600	60	$2D$	10
RW2L3N3	300	200	$4D$	3

2.1 Design and Capabilities

To give the microrobot as much torque as possible for actuation different configurations were designed. These designs differ from each other in geometry, number and shape of soft-magnetic posts and their configuration in the device. Geometrically, these microrobots were fabricated with different length l and width w of the body. The configuration of the soft-magnetic posts varies in pitch between the posts d_p, the number of posts n_p as well as the shape (cylindrical or rectangular). All cylindrical soft-magnetic posts have a diameter $D = 30\,\mu\text{m}$ and a height of $h = 50\,\mu\text{m}$. Several configurations are detailed in Fig. 4.1 and their type name is explained in Table 4.1. For example, a microrobot with length $l = 300\,\mu\text{m}$, width $w = 60\,\mu\text{m}$, number of posts $n_p = 5$, spaced $d_p = 2D$ apart, would be denoted as RL3N5.

According to [17], the torque can be increased with either a stronger magnetic field $\mathbf{H}$, a more pronounced easy axis, or with increasing volume V of the magnetic material. The limitation of increasing magnetic material is related to the preferred magnetization direction (easy axis) of the device. In order to achieve the desired rolling motion (left two designs in Fig. 4.1) the microrobot has to be kept as symmetrical as possible along its long axis and has a transverse magnetization. This is achieved with the internal soft-magnetic posts. When the pitch between the soft-magnetic posts d_p is too small, the magnetization direction can change. The ideal configuration, therefore, depends on d_p, and defines the number of posts n_p. For increasing pitch distance d_p the soft-magnetic posts do not influence each other and behave like individual cylinders. The minimal configuration was experimentally found with $d_p = 2D$. The dimensions of the soft-magnetic posts are therefore preferred with a diameter of $D = 30\,\mu\text{m}$ and a height of $h = 50\,\mu\text{m}$, thus having a height to diameter ratio of $h/D \approx 1.67$. This leads to a volume fraction of CoNi in the device up to 20 % (nearly 65 % by weight) allowing a high magnetization and generating sufficient torque to drive the agent in liquid environments, including in higher viscosity fluids.

Regarding the stepping actuation technique of the device (right design in Fig. 4.1), the microrobot is designed as a rectangular cuboid, with internal rectangular soft-magnetic posts. This leads to a height to diameter ratio of $h/D \approx 2.92$ offering sufficient torque to enable the stepping actuation technique. For both designs, motion is induced due to the friction of the microrobot with the supporting surface, which is explained in more detail in Sect. 3.

2.2 Fabrication

For the fabrication of the microrobot, a silicon wafer covered with a silicon dioxide (SiO_2) sacrificial layer is used as the substrate, followed by an evaporated titanium (Ti) and gold (Au) bilayer that is patterned by a lift-off process. A thin layer of adhesion promoter, Omnicoat, and a 50 μm thick layer of SU-8 are spincoated on the wafer and patterned into tethered structures with holes within the bodies. The holes are then filled with CoNi alloy by an electroplating process, followed by another thin layer of electroplated gold to protect the CoNi alloy during the subsequent etching step. The wafer is then diced into small chips and immersed in a buffered hydrofluoric (BHF) acid solution to etch away SiO_2 and release the structures from the substrate. Finally, a micro-laser milling machine is utilized to cut the microrobots from their tethers. For more details on the fabrication process, we refer to [21]. This fabrication procedure lends itself perfectly for mass-production of the microrobot and in one batch (wafer) up to 40,000 devices can be fabricated.

Due to its exceptional magnetic properties, electrodeposited soft-magnetic cobalt-nickel (CoNi) is used. The content ratio of cobalt and nickel specifies the magnetic properties of the material. This leads to tunable magnetic properties, ranging from semi-hard to very soft [22]. The used CoNi alloy contains approximately 50 % Co and has high magnetic permeability, high magnetic saturation and low remanence [a saturation magnetization of 0.85 T, and a coercivity of 20 Oe (0.002 T)]. The high magnetic permeability allows the magnetic material to generate higher force or torque in a stronger external magnetic field. A low remanence reduces the residual magnetic force when the magnetic field is turned OFF?

3 Magnetic Actuation

Actuation with magnetic fields is a convenient method for applying power to a microrobot and control its motion. Considering a magnetic field $\mathbf{H}$ that is applied in the workspace, the magnetic torque and force that is acting on the microrobot can be defined as

$$\boldsymbol{\tau} = V\mathbf{M} \times \mathbf{B} \tag{4.1}$$

where $\mathbf{M}$ is the volume magnetization in $[A/m]$ of the object of volume V, the magnetic field has a flux density $\mathbf{B} = \mu_0\mathbf{H}$ and μ_0 is the permeability of vacuum. The force acting on the microrobot is described as

$$\mathbf{F} = V(\mathbf{M} \cdot \nabla)\mathbf{B}. \tag{4.2}$$

For the designs presented in this work, the device is actuated by magnetic torque.

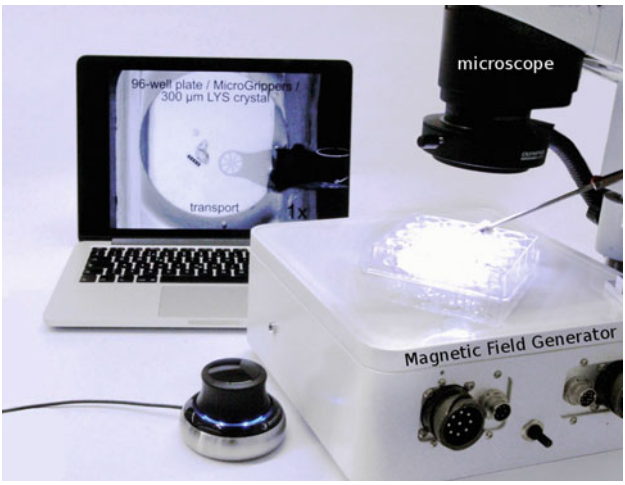

Fig. 4.2 The experimental system contains the eight-coil magnetic field generator (MFG, white box), a microscope (Olympus IX-81) and a laptop computer for user interaction. Image courtesy of MagnebotiX AG

3.1 Experimental System

The magnetic field generator (MFG) has eight electromagnetic coils as described in [23] and is commercialized by MagnetbotiX AG[1]. The system is controlled by a single computer and is capable of 5-DOF wireless control of micro- and nano-structures (3-DOF position, 2-DOF pointing orientation) within a spherical workspace with a diameter of approximately 10 mm. This allows for magnetic fields and field gradients up to 20 mT and 2 T/m. The MFG is positioned under a microscope (Olympus IX-81) to observe a container enclosing the microrobot (see Fig. 4.2). For all experiments the magnitude of the magnetic field is set to 10 mT and, as the motion of all presented devices is torque induced, no magnetic field gradient is applied.

3.2 Rotational Magnetic Fields

Figure 4.3 describes the motion of a rolling microrobot actuated with a rotating magnetic field. If the microrobot rolls without slipping, the maximum forward velocity can be determined as $\hat{v}_{\text{com},r} = 2 \cdot (w + h) \cdot \omega$, with ω the rotational frequency of the magnetic field. This assumes that the robot follows the field exactly. The forward body length of the microrobot is $w = 60\,\mu\text{m}$, resulting in

[1] http://www.magnebotix.com

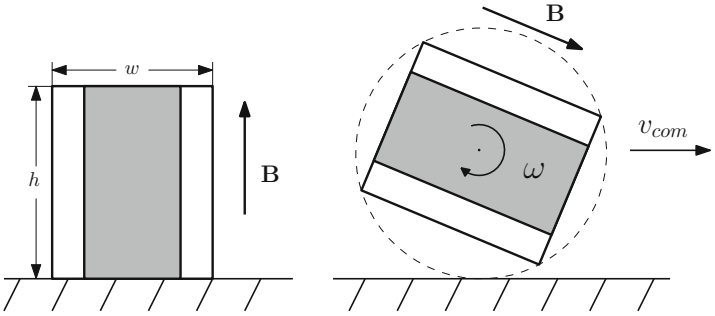

Fig. 4.3 Side view of a microrobot capable of rolling motion. Applying a rotational magnetic field **B** enables the microrobot to roll on a supporting surface with a rotational velocity ω and results in a forward motion v_{com}

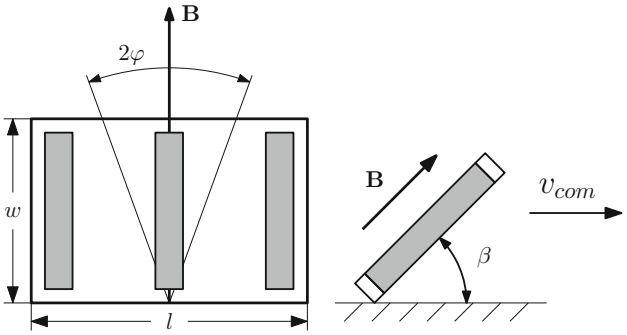

Fig. 4.4 Top view (*left*) and side view (*right*) of a microrobot capable of stepping motion. Applying a stepping magnetic field **B** enables the microrobot to tilt and slide on a supporting surface and results in a forward motion v_{com}. φ represents the stepping angle and β represents the tilt angle of the magnetic field

a forward velocity of around 16 body lengths/s at a rotation frequency of 5 Hz. The deviation of the experimental data from this ideal forward velocity indicates slip of the microrobot, as will be explained in Sect. 3.4.

3.3 Stepping Magnetic Fields

Figures 4.4 and 4.5 show the motion of a microrobot of type RW2L3N3 actuated with a stepping magnetic field. If the microrobot steps without slipping, the maximum forward velocity can be determined as $\hat{v}_{\text{com},s} = l \sin(\phi) \cdot \eta$, with η the stepping frequency of the magnetic field. The forward body length of the microrobot is $w = 200\,\mu\text{m}$, resulting in a forward velocity of around 2.5 body lengths/s at a stepping frequency of 5 Hz. The forward velocity does not depend on the tilt angle

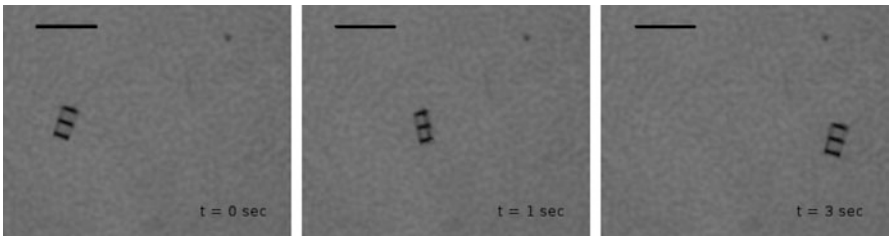

Fig. 4.5 Snapshots of microrobot actuation via a stepping magnetic field. The microrobot of type RW2L3N3 ($l = 300\,\mu$m, $w = 200\,\mu$m) moves from left to right and covers a distance of approximately 1.6 mm in the images sequence. This results in a forward speed of around 2.5 body lengths/s. The black scale bar is 500 μm long

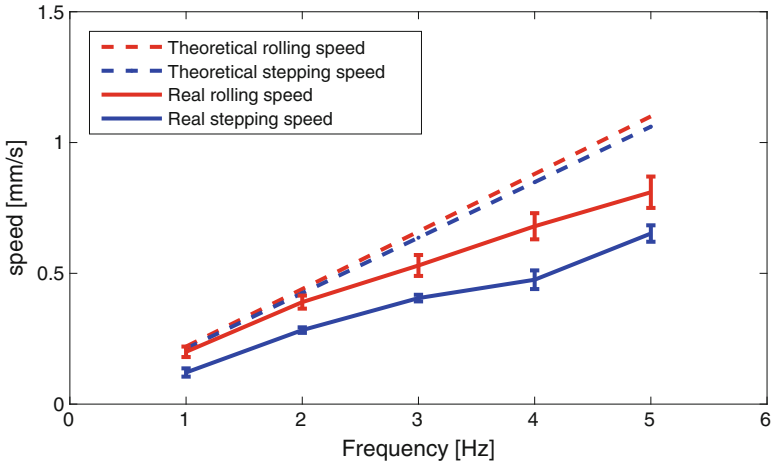

Fig. 4.6 Theoretical (*dashed lines*) and real (*solid lines*) forward speed for the rolling (*red lines*) and stepping (*blue lines*) locomotion technique. The real speed is obtained with water (rolling) and isopropanol (stepping) as liquid environment. For the stepping locomotion technique the microrobot's length is $l = 300\,\mu$m, the stepping angle $\phi = 45\,^\circ$ and the tilt angle of the magnetic field $\beta = 40\,^\circ$. Each measurement is averaged over three experiments and the error bar represents one standard deviation

β of the magnetic field, and was set to $\beta = 40\,^\circ$. The deviation of the experimental data from this ideal forward velocity indicates slip of the microrobot, as will be explained in the next section.

3.4 Evaluation

Figure 4.6 shows the theoretical (dashed lines) and real (solid lines) forward speed for the rolling (red lines) and stepping (blue lines) locomotion technique. For the rolling experiments a microrobot of type RL6N10 is used, while for the stepping

experiments a microrobot of type RW2L3N3 is used. The stepping locomotion is evaluated with a stepping angle of $\phi = 45°$ and a tilt angle of the magnetic field $\beta = 40°$. Because the experimental velocity is lower than the theoretical speed, slip of the microrobot limits the forward speed. One reason for this slip is the viscosity of the surrounding liquid, i.e. when the viscosity is higher this leads to more slip and a lower velocity [20]. Additionally, as forward motion is achieved due to the frictional contact between the microrobot and the surface, the roughness of the supporting surface plays a role as well. When the surface roughness is high, the microrobot is expected to have more traction than for a smooth surface, and the resulting forward speed will be higher. These explanations hold for both the rolling and stepping actuation technique. The motion of the microrobots was evaluated in water (rolling) and isopropanol (stepping) on a glass substrate.

4 Object Manipulation

The properties of the environment prescribe which object manipulation techniques are possible. Considering a liquid environment, the density and viscosity of the liquid, as well as the density of the object, dictate whether an object can be lifted or not. For example, the density of polystyrene ($1.05\,\mathrm{kg\,m^{-3}}$) is higher than the density of isopropanol ($0.79\,\mathrm{kg\,m^{-3}}$, at room temperature). This ensures a polystyrene bead will sink in isopropanol due to gravity, but can still be lifted up due to a generated fluid flow. This delicate balance between the properties of the object and the surrounding fluid demonstrates the importance of environmental conditions and enables two manipulation capabilities. First, manipulation via direct contact is shown, where the microrobot pushes an object. Second, the motion of the rolling microrobot can generate a local fluidic vortex which enables a noncontact manipulation technique.

4.1 Contact Manipulation

Object manipulation by pushing is a common strategy for microrobots and is possible when the object to be manipulated is heavy enough as not to be lifted by the fluid flow and light enough such that the microrobot can actually move it. This means that the apparent weight of the object, and the electrostatic and the Van der Waals forces due to the interaction of the object with the surface, must be lower than the force applied by pushing. Figure 4.7 shows a microrobot of type RW2L3N3 (300 μm wide) pushing a micro-object (200×350 μm) that is triangular shaped and is fabricated from SU-8 (density $1.2\,\mathrm{kg\,m^{-3}}$). Figure 4.8 shows a microrobot of type RL3N5 pushing four micro-objects (SU-8 triangles, 200×350 μm) such that they densely assemble into a narrow channel (750 μm wide). Pushing manipulation is more effective with a rolling microrobot than with a stepping microrobot. This is because the stepping actuation technique achieves less stable motion than the

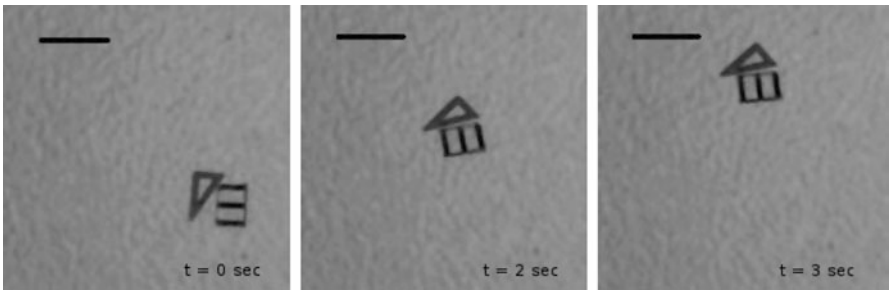

Fig. 4.7 Microscopic view of object manipulation via pushing. The microrobot of type RW2L3N3 (300 μm wide) pushes a micro-object (SU-8 triangle, 200×350 μm). The black scale bar is 500 μm long

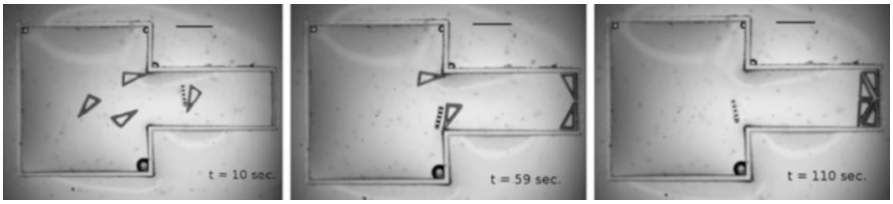

Fig. 4.8 Microscopic view of object manipulation via pushing. The microrobot of type RL3N5 (300 μm wide) assembles four micro-objects (SU-8 triangles, 200 × 350 μm) densely packed into a narrow channel (750 μm wide) within 2 min. The black scale bar is 500 μm long

rolling technique, and the orientation of the device can be better controlled with rolling. The orientation of the stepping microrobot is continuously stepping in order to move forward which works against a continuous and stable pushing contact.

4.2 Noncontact Manipulation

The lifting effect of the fluid flow in front of the microrobot and near the surface occurs due to the no-slip condition of the fluid at the surface (shear flow) and causes objects to be lifted up from the surface. This fluidic lifting effect is local, as objects further away from the robot are not affected. The fluidic vortex above the microrobot is generated due to the robot's rotation and the fluid's no-slip condition at the surface. Both effects complement each other, and are possible due to the low Reynolds number environment [24]. Figure 4.9 shows a microrobot of type RL6N10 (600 μm wide) lifting and transporting a polystyrene bead that is 100 μm in diameter.

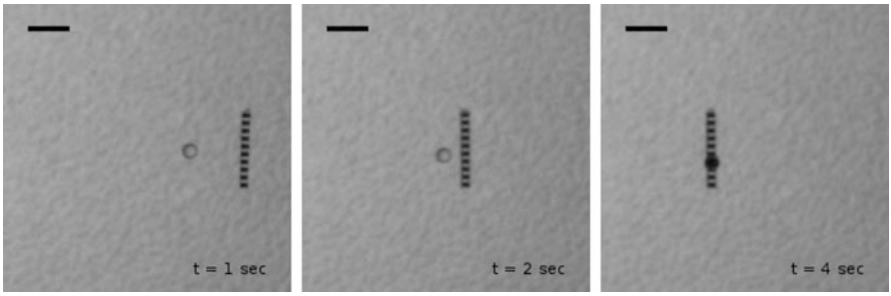

Fig. 4.9 Microscopic view of object manipulation via fluidic trapping. The microrobot of type RL6N10 (600 μm wide) approaches (*left*), lifts (*middle*) and transports (*right*) a polystyrene bead with 100 μm in diameter. The black scale bar is 300 μm long

5 Conclusions

This chapter presented the design and capabilities of a family of microrobots. While the fabrication process is identical for all designs, the method for actuation and the object manipulation capabilities are specific for each particular design. Each microrobot design has embedded soft-magnetic posts that align to a magnetic field. Depending on the arrangement of these posts the microrobot can be actuated by either a rotating magnetic field or a stepping magnetic field. Consequently, each actuation technique enables a different object manipulation techniques (i.e. contact or noncontact manipulation). In particular, a rotating magnetic field enables a local vortex above the robot that traps objects for transportation. Moreover, a pushing manipulation technique can be achieved for both the rotating and stepping magnetic field actuation. Experimental results demonstrate all mentioned techniques for different microrobotic designs.

References

1. Abbott J, Nagy Z, Beyeler F, Nelson B (2007) Robotics in the small, part I: microbotics. IEEE Robot Autom Mag 14(2):92–103
2. Purcell E (1977) Life at low Reynolds number. Am J Phys 45(1):3–11
3. Abbott JJ, Peyer KE, Cosentino Lagomarsino M, Zhang L, Dong LX, Nelson BJ (2009) How should microrobots swim? Int J Robot Res 28(11–12):1434–1447
4. Sun Y, Liu X (2015) Micro- and nanomanipulation tools. Wiley, New York
5. Bouchebout S, Bolopion A, Abrahamians J-O, Régnier S (2012) An overview of multiple DoF magnetic actuated micro-robots. J Micro-Nano Mechatronics 7(4):97–113
6. Xu T, Yu J, Yan X, Choi H, Zhang L (2015) Magnetic actuation based motion control for microrobots: an overview. Micromachines 6:1346–1364
7. Banerjee A, Gupta S (2013) Research in automated planning and control for micromanipulation. IEEE Trans Autom Sci Eng 10(3):485–495

8. Savia M, Koivo H (2009) Contact micromanipulation - survey of strategies. IEEE/ASME Trans Mechatronics 14(4):504–514
9. Kummer M, Abbott J, Kratochvil B, Borer R, Sengul A, Nelson B (2010) Octomag: An electromagnetic system for 5-DOF wireless micromanipulation. IEEE Trans Robot 26(6), 1006–1017
10. Bergeles C, Kratochvil B, Nelson B (2012) Visually servoing magnetic intraocular microdevices. IEEE Trans Robot 28(4):798–809
11. Frutiger DR, Vollmers K, Kratochvil BE, Nelson BJ (2009) Small, fast, and under control: wireless resonant magnetic micro-agents. Int J Robot Res 29:613–636.
12. Pawashe C, Floyd S, Diller E, Sitti M (2012) Two-dimensional autonomous microparticle manipulation strategies for magnetic microrobots in fluidic environments. IEEE Trans Robot 28(2):467–477
13. Steager EB, Sakar MS, Magee C, Kennedy M, Cowley A, Kumar V (2013) Automated biomanipulation of single cells using magnetic microrobots. Int J Robot Res 32:346–359
14. Nelson BJ, Kaliakatsos IK, Abbott JJ (2010) Microrobots for minimally invasive medicine. Ann Rev Biomed Eng 12:55–85
15. Crane NB, Onen O, Carballo J, Ni Q, Guldiken R (2012) Fluidic assembly at the microscale: progress and prospects. Microfluid Nanofluid 14(3):383–419
16. Floyd S, Pawashe C, Sitti M (2009) Two-dimensional contact and noncontact micromanipulation in liquid using an untethered mobile magnetic microrobot. IEEE Trans Robot 25(6):1332–1342
17. Pieters RS, Tung H-W, Charreyron S, Sargent SF, Nelson BJ (2015) RodBot: a rolling microrobot for micromanipulation. In: Proceedings of IEEE international conference on robotics and automation (ICRA), pp 4042–4047
18. Happel J, Brenner H (1983) Low Reynolds number hydrodynamics: with special applications to particulate media. Martinus Nijhoff, The Hague
19. Bhushan B (1998) Handbook of micro/nano tribology. CRC Press, Boca Raton
20. Tung H-W, Peyer KE, Sargent DF, Nelson BJ (2013) Noncontact manipulation using a transversely magnetized rolling robot. Appl Phys Lett 103(11):114101
21. Tung H-W, Sargent DF, Nelson BJ (2014) Protein crystal harvesting using the RodBot - a wireless, mobile microrobot. J Appl Crystallogr 4:692–700
22. Ergeneman O, Sivaraman KM, Pané S, Pellicer E, Teleki A, Hirt AM, Baró MD, Nelson BJ (2011) Morphology, structure and magnetic properties of cobalt nickel films obtained from acidic electrolytes containing glycine. Electrochim Acta 56(3):1399–1408
23. Kratochvil BE, Kummer MP, Erni S, Borer R, Frutiger DR, Schürle, S, Nelson BJ (2014) MiniMag: a hemispherical electromagnetic system for 5-DOF wireless micromanipulation. In Khatib O, Kumar V, Sukhatme G (eds) Experimental Robotics. Springer Tracts in Advanced Robotics, vol 79. Springer, Berlin, pp 317–329
24. Merlen A, Frankiewicz C (2011) Cylinder rolling on a wall at low Reynolds numbers. J Fluid Mech 685:461–494